

Chapter 16

Encircled Energy

Diab Jerius

In this chapter we present a set of encircled energy curves, measured at various energies and for various mirror combinations.

The experiments and data reductions were described in Chapter 12 and Chapter 9, respectively. We present here plots of the effective area captured within a circular aperture centered on the focused image, as functions of the aperture diameter.

Some of the experiments were done one shell at a time, on axis, at the C K- α , Al K- α , Ti K- α , and Fe K- α lines. Also done on-axis were full-HRMA measurements at the Cu L- α , Cr K- α , and Cu K- α lines. In addition, there were “ends survey” tests done, in which one quadrant of a single mirror shell was exposed, and the HRMA tilted in pitch or yaw to simulate an infinite source distance. This illuminates a larger fraction of the length of the optic, and allows one to search for effects of larger surface roughness near the ends of the optic.

A few encircled energy tests were done with the solid state detectors, both with the continuum source (EIPS with graphite target, 15 kV, and a beryllium target), and with selected lines such as Ag and Sn L- α . The analysis of these data lag behind the simpler FPC spectra, and are not reported here.

The natural units for the measured points in an encircled energy experiment are cm^2 , since the measured quantity is the effective area, integrated over the aperture. There are occasional points where, due to experimental error, the error bars are large and the points lie off the trend line. In most cases these points are within the calculated error bar of the trend line, so few real excursions exist. Those excursions which are real are cases in which the aperture was not properly centered on the image, and so the flux measured in the pinhole is less than it should have been. These points should be ignored.

Current ray trace models do not yet incorporate an accurate image of the source’s spatial structure, and so are not comparable to the data. The source is believed to subtend an angle of $0.2''$ or so as seen from the HRMA, and so the core of the image is somewhat more diffuse than the point-source ray trace models predict. The normalization of the curves are also somewhat discrepant. This effect is discussed elsewhere in this document, in the chapters on effective areas (Chapter 12 and Chapter 11). However, except for the inner core of the image, the shapes of the encircled energy curves match the simulations quite closely.

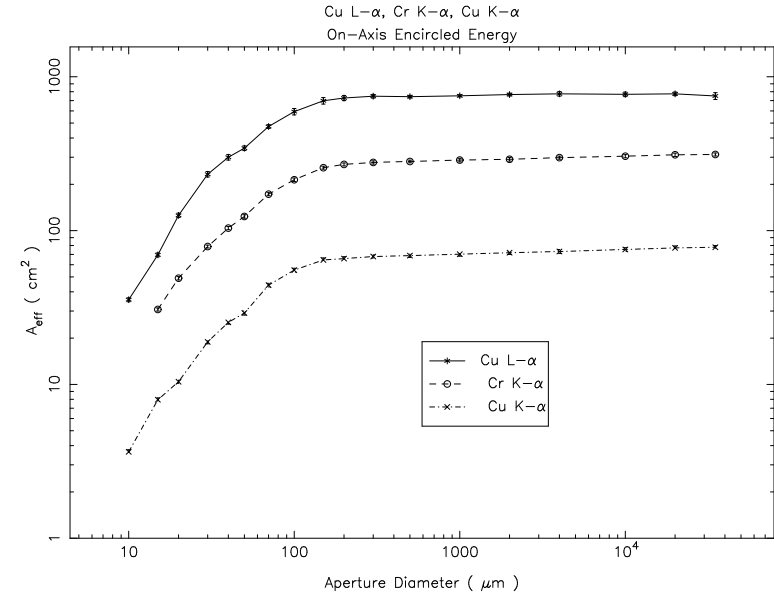


Figure 16.1: On-axis Full-HRMA Copper L- and K- α and Chromium K- α Encircled Energy

16.1 Comparison of Encircled Energy Measurements to Simulations

Figures 16.4 to 16.8 show comparisons of the measured FPC encircled energies to the simulations. In general the agreement is quite good. The inner cores disagree in part because the simulations treat the XSS as a point source. Additionally, the smaller pinholes were not reliably centered.

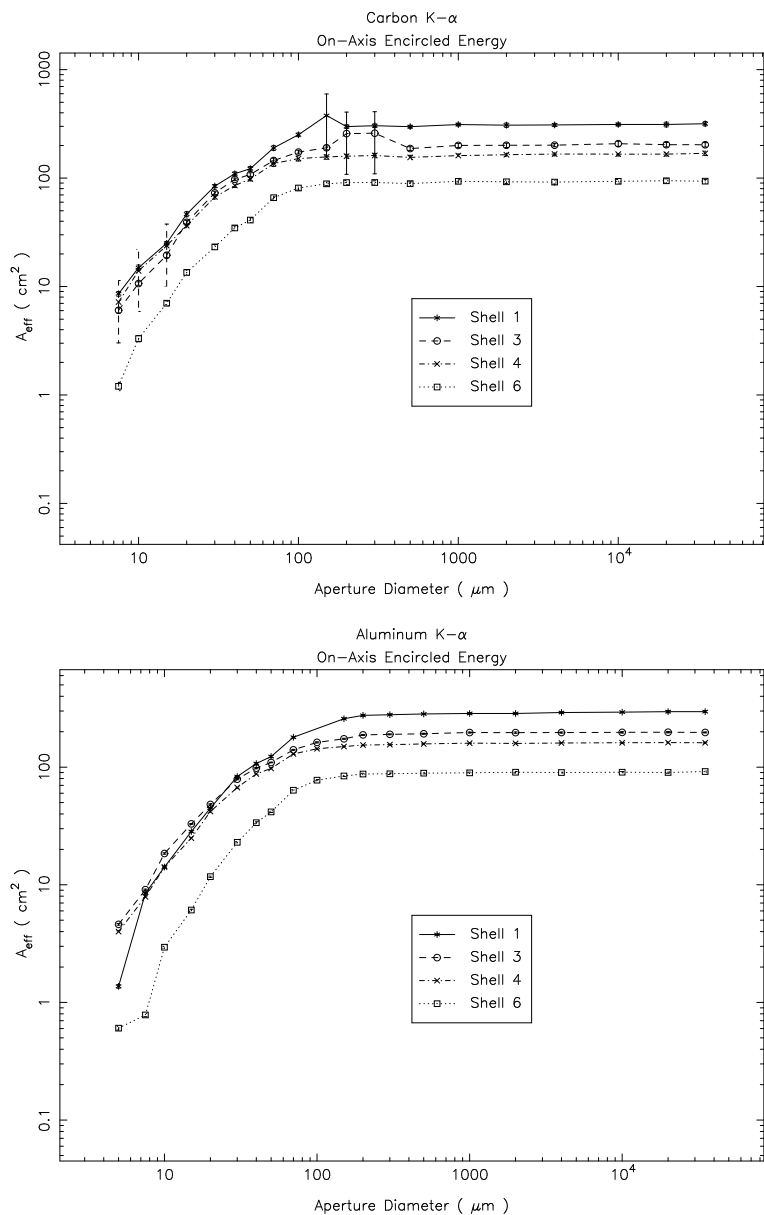


Figure 16.2: On-axis Carbon and Aluminum K- α Encircled Energy

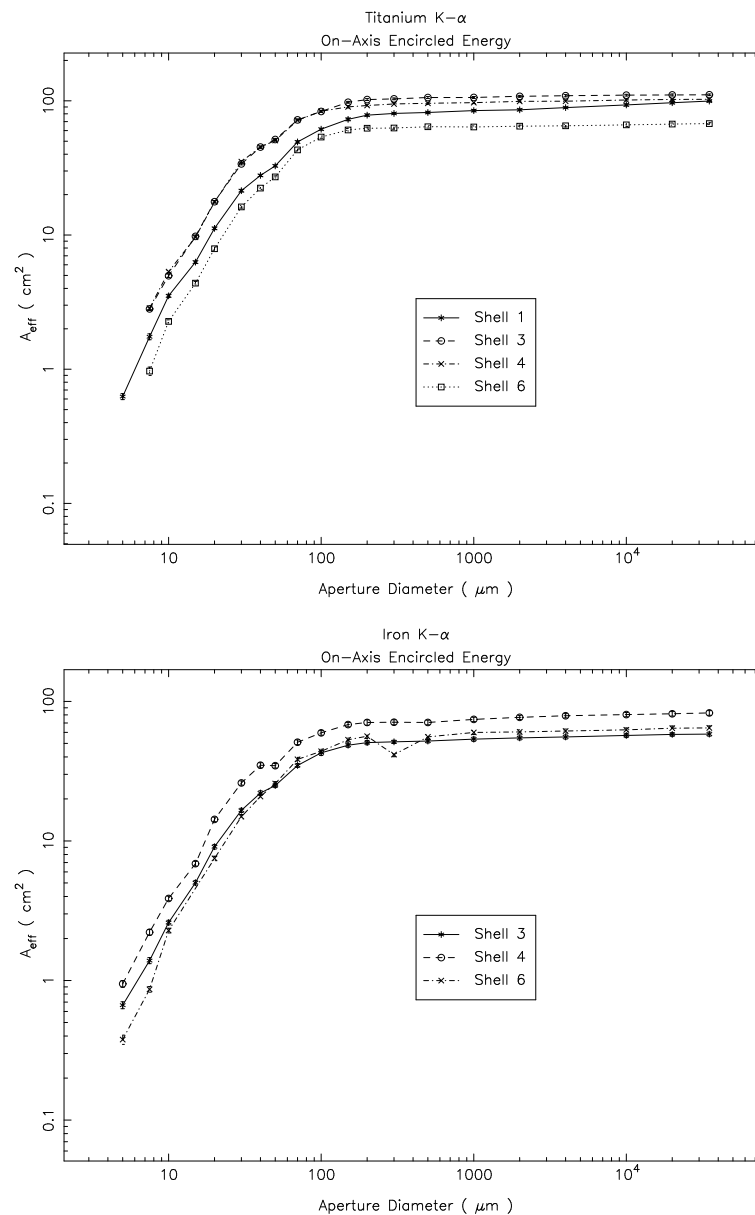


Figure 16.3: On-axis Titanium and Iron K- α Encircled Energy

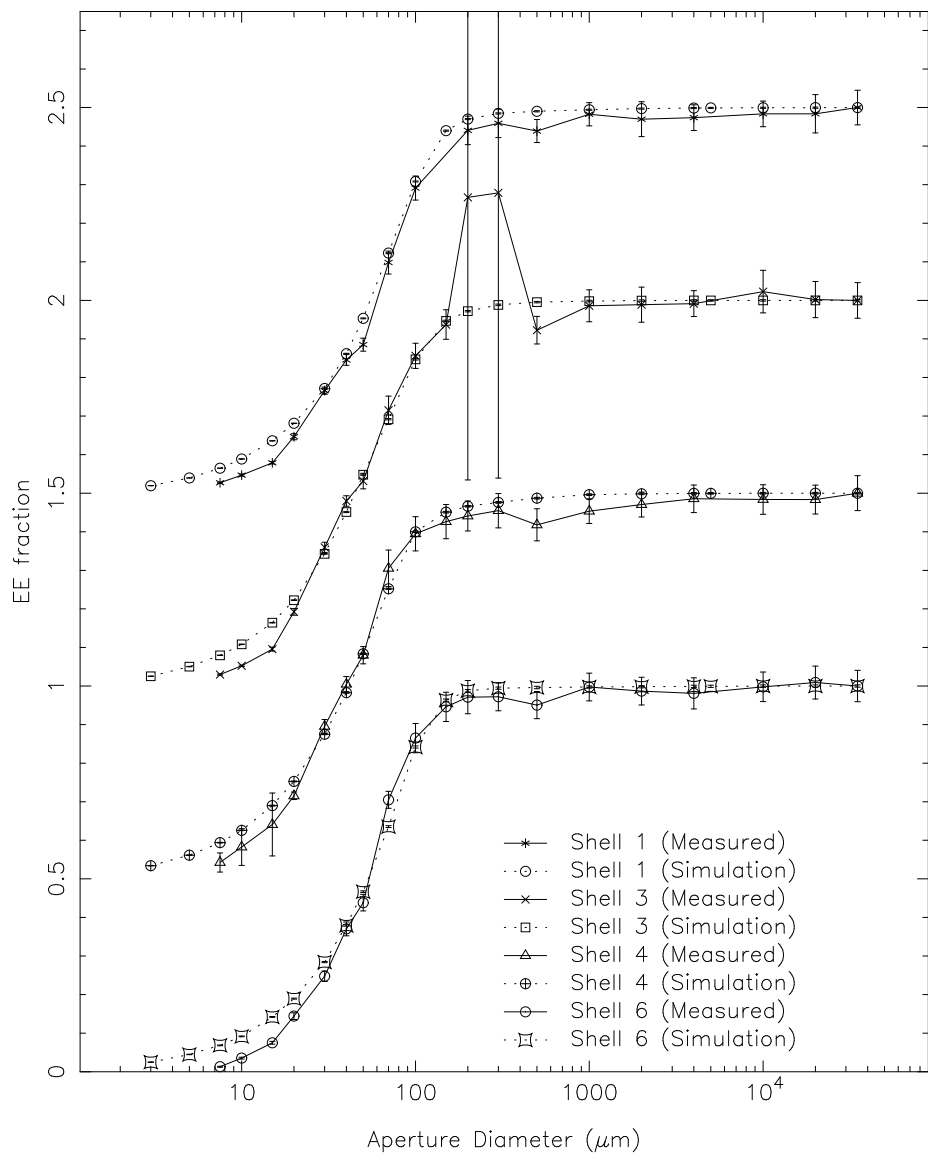


Figure 16.4: Encircled Energy Fractions at 0.277 keV. The values for Shells 1–3 have been shifted upwards for clarity.

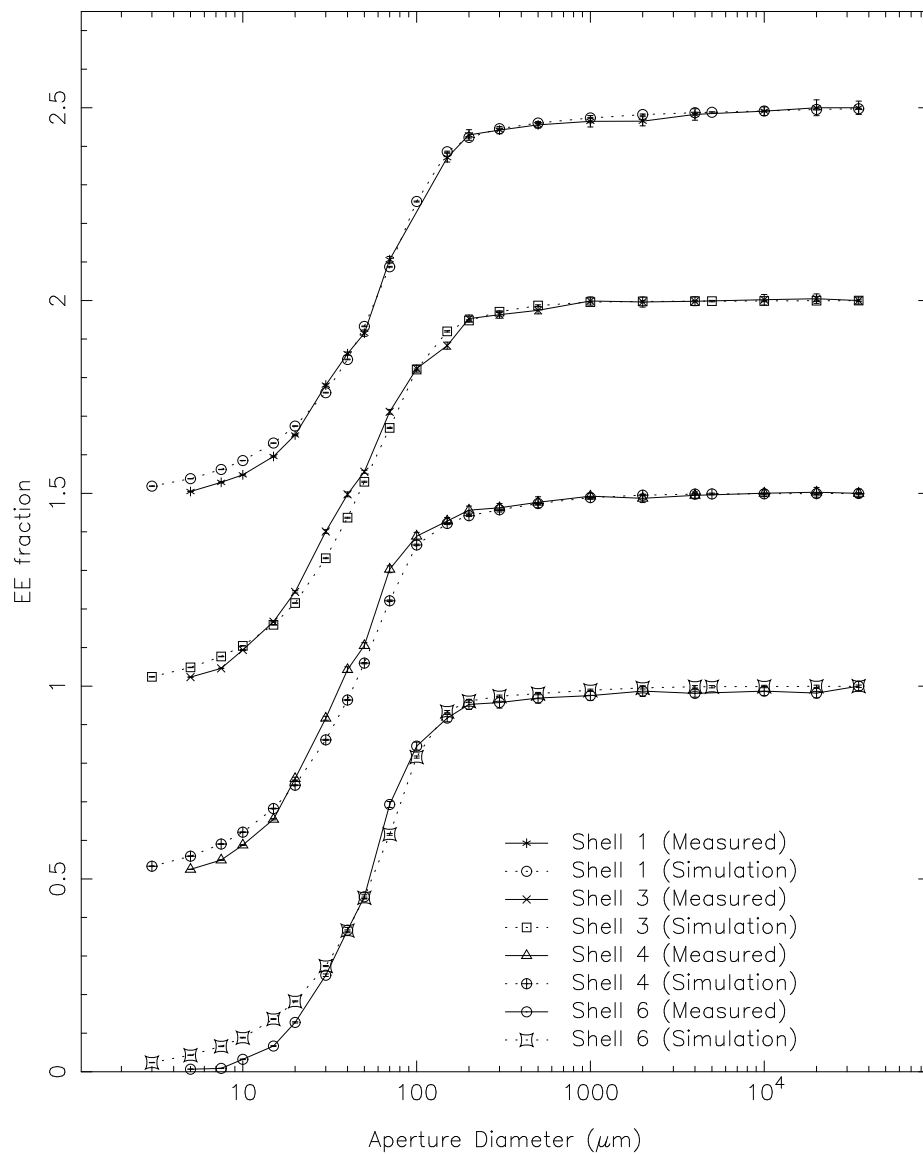


Figure 16.5: Encircled Energy Fractions at 1.486 keV. The values for Shells 1–3 have been shifted upwards for clarity.

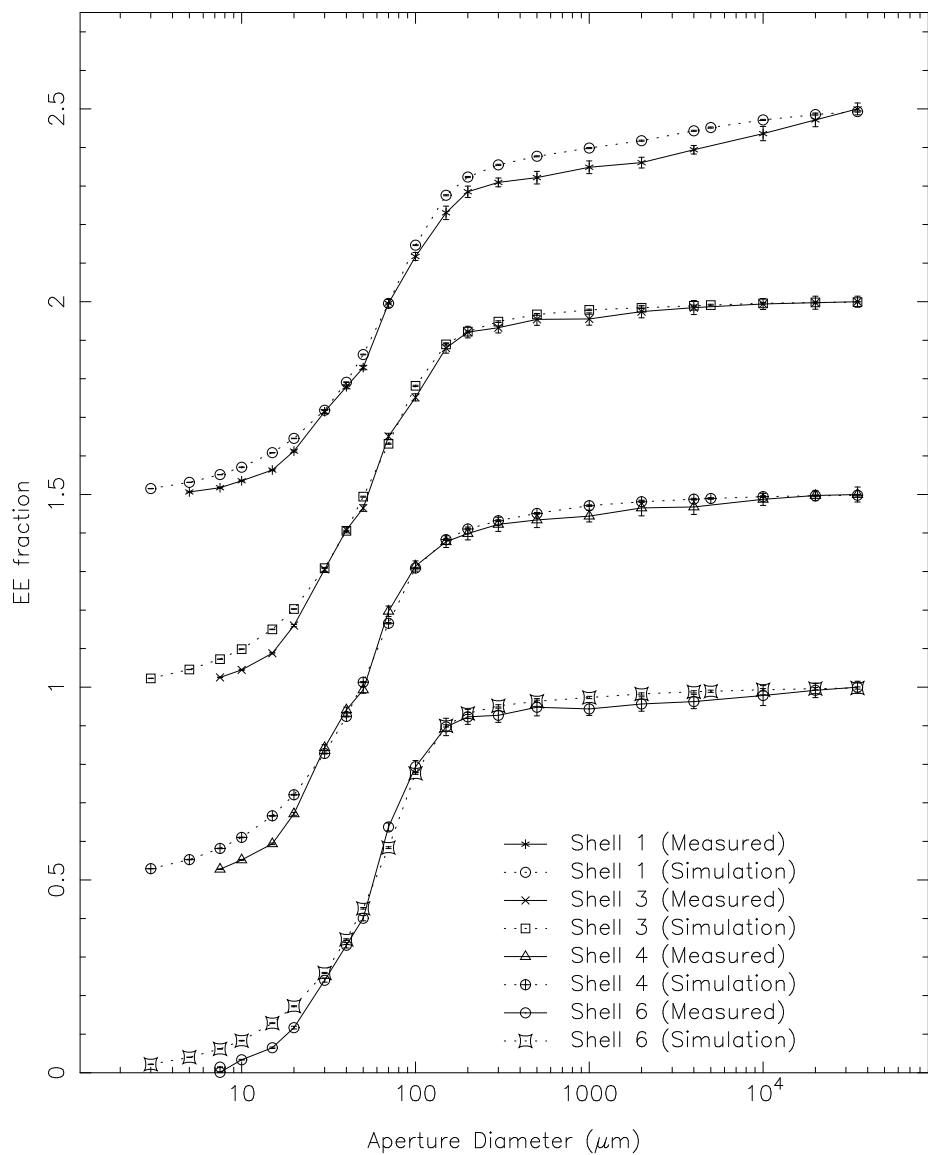


Figure 16.6: Encircled Energy Fractions at 4.51 keV. The values for Shells 1–3 have been shifted upwards for clarity.

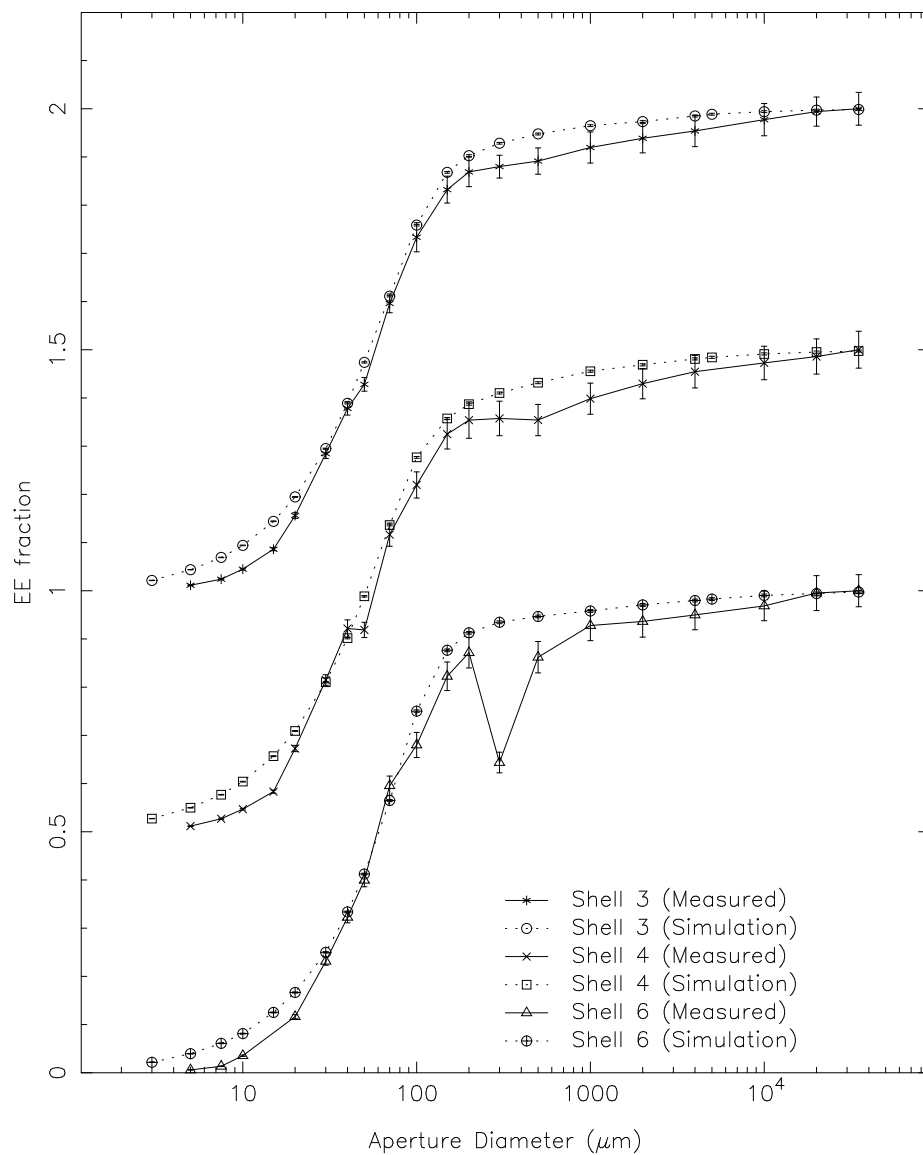


Figure 16.7: Encircled Energy Fractions at 6.4 keV. The values for Shells 3 and 4 have been shifted upwards for clarity.

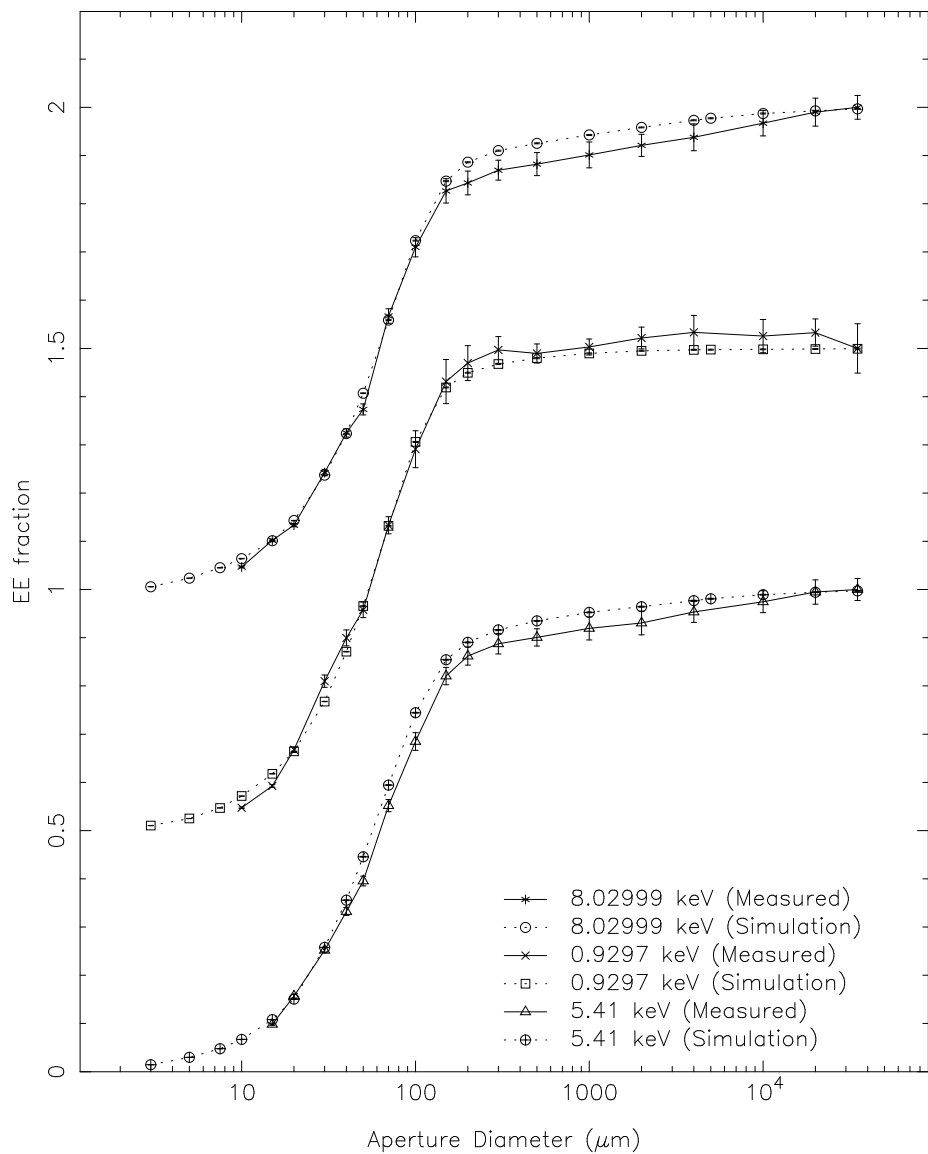


Figure 16.8: HRMA Encircled Energy Fractions. The values for higher energies have been shifted upwards for clarity.